Supporting Information

$Ti_3C_2T_x$ MXene/Alginic Acid-Derived Mesoporous Carbon Nanocomposite as a Potential Electrode Material for Coin-Cell Asymmetric Supercapacitor

Sanjay D. Sutar, and Anita Swami*

Department of Chemistry, SRM Institute of Science and Technology, Kattankulathur - 603 203, Chennai (India)

*Corresponding author e-mail: swamians@srmist.edu.in

Instrumental Characterization

The $Ti_3C_2T_x$/Mesoporous Carbon nanocomposites were characterized using various spectroscopic and microscopic techniques. Powder XRD patterns were recorded on an X'pert pro diffractometer, PANalytical using Cu K_α radiation (λ = 1.5406 Å, 40 kV, 40 mA) in the 2θ range of 5-90° with the scan rate of 2° min^{-1}. Micro-Raman Spectrometer (LabRAM HR Evolution HORIBA France) was used for Raman analysis, using powder samples on a glass substrate. An oxxius laser of 633 nm wavelength (having max. power of 100 mW) was used throughout the complete measurement. The morphology of the prepared nanocomposites was investigated by using scanning electron microscopy (SEM) on a Quanta 200 FEG FE-SEM and transmission electron microscopy (TEM) on a JEOL-1010 transmission electron microscope operated at an acceleration voltage of 20 kV and 100 kV respectively. Whereas, high angle annular dark field-scanning transmission electron microscopy (HAADF-STEM) and elemental analysis mapping were conducted on an FEI make Tecnai TEM T-20 operating at 200 kV with LaB_6 filament fitted with Gatan Digital camera (bottom mount) with a resolution of 2K. The specific surface area of the sample was calculated by the Brunauer-Emmet-Teller (BET) method using a Quantachrome Nova-1000 surface analyzer. The pore size distribution was determined from the adsorption branches of isotherms through Barrett-Joyner-Halenda (BJH) method. Thermo Gravimetric Analysis (TGA) were done with a STA 2500 Regules instrument at a temperature range, RT-1100 °C in an inert atmosphere. X-ray photoelectron spectroscopy (XPS) measurements were done with a Thermo K-5 Alpha XPS instrument at a pressure better than 1×10^{-9} Torr with a pass energy of 50 eV, electron take-off angle of 60° and an overall resolution of ~1 eV using monochromatic Al K_α (source, hν = 1486.6 eV). The spectra were fitted using a combined polynomial and Shirley-type background function.

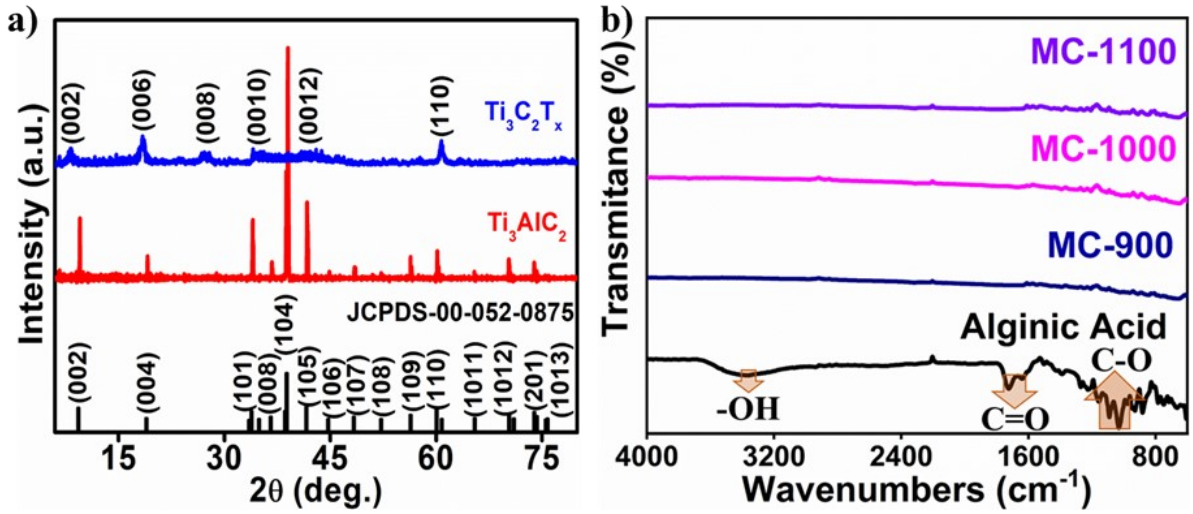

Figure S1. (a) XRD patterns of Ti_3AlC_2 and $Ti_3C_2T_x$; (b) FTIR spectra of the Alginic acid and MC-T.

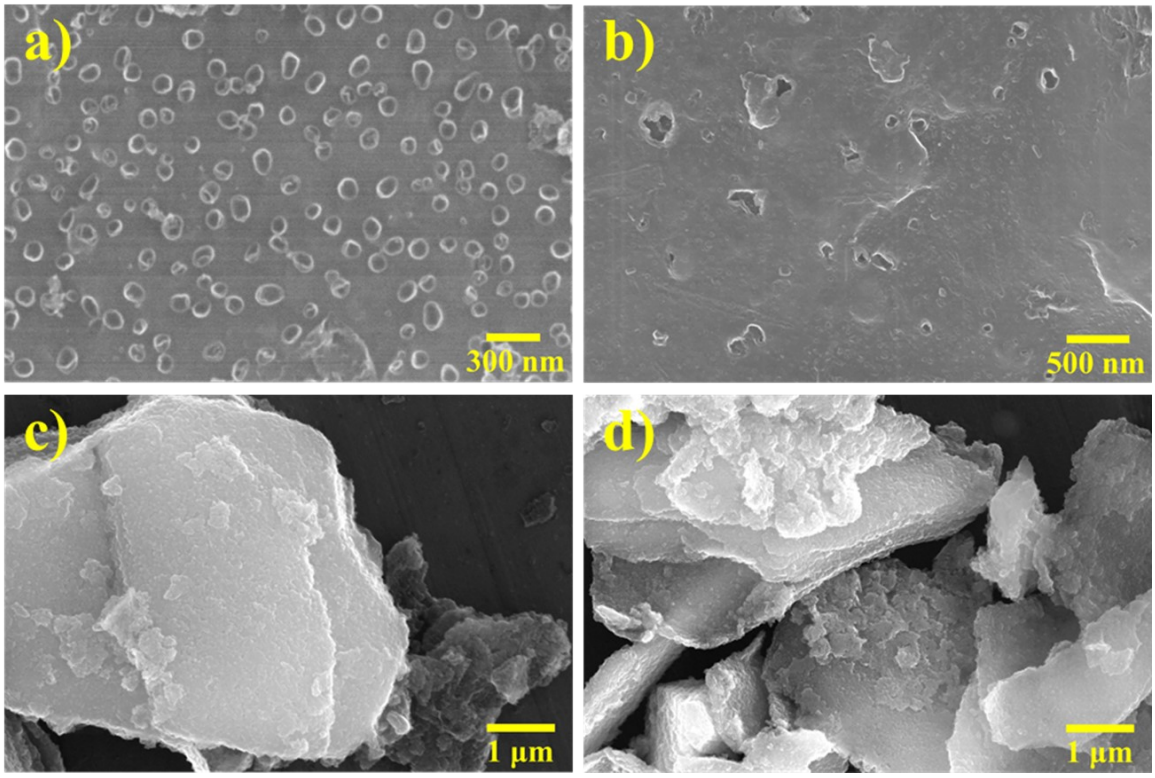

Figure S2. SEM images of (a) MC-900, (b) MC-1100, (c) $Ti_3C_2T_x$/MC-5 and (d) $Ti_3C_2T_x$/MC-1 nanocomposite.

Table S1. Titanium, Carbon, Oxygen and Fluorine content (wt% and at%) obtained from EDS analysis of all synthesized materials

Materials	Carbon		Oxygen		Titanium		Fluorine	
	Wt %	**At %**	**Wt %**	**At %**	**Wt %**	**At %**	**Wt %**	**At %**
Alginic Acid	47.6	54.7	52.4	45.3				
MC-900	83.7	84.1	16.3	15.9				
MC-1000	88.5	88.7	11.5	11.3				
MC-1100	87.8	86.5	13.2	13.5				
$Ti_3C_2T_x$	15.8	16.0	2.9	4.0	66.6	63.0	14.7	17.0
$Ti_3C_2T_x$/MC-9	78.1	77.2	17.5	16.8	3.1	3.8	1.3	2.2
$Ti_3C_2T_x$/MC-5	43.6	46.1	19.6	19.4	30.1	29.2	6.7	5.3
$Ti_3C_2T_x$/MC-1	9.2	10.1	25.6	27.1	56.4	53.2	8.8	9.6

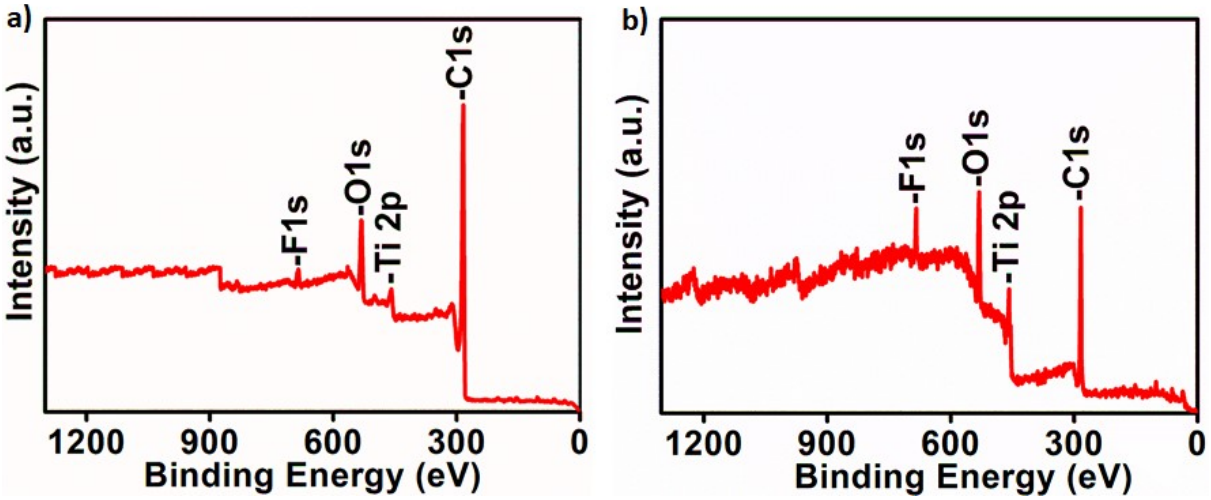

Figure S3. XP survey spectra of $Ti_3C_2T_x$/MC-9 and $Ti_3C_2T_x$.

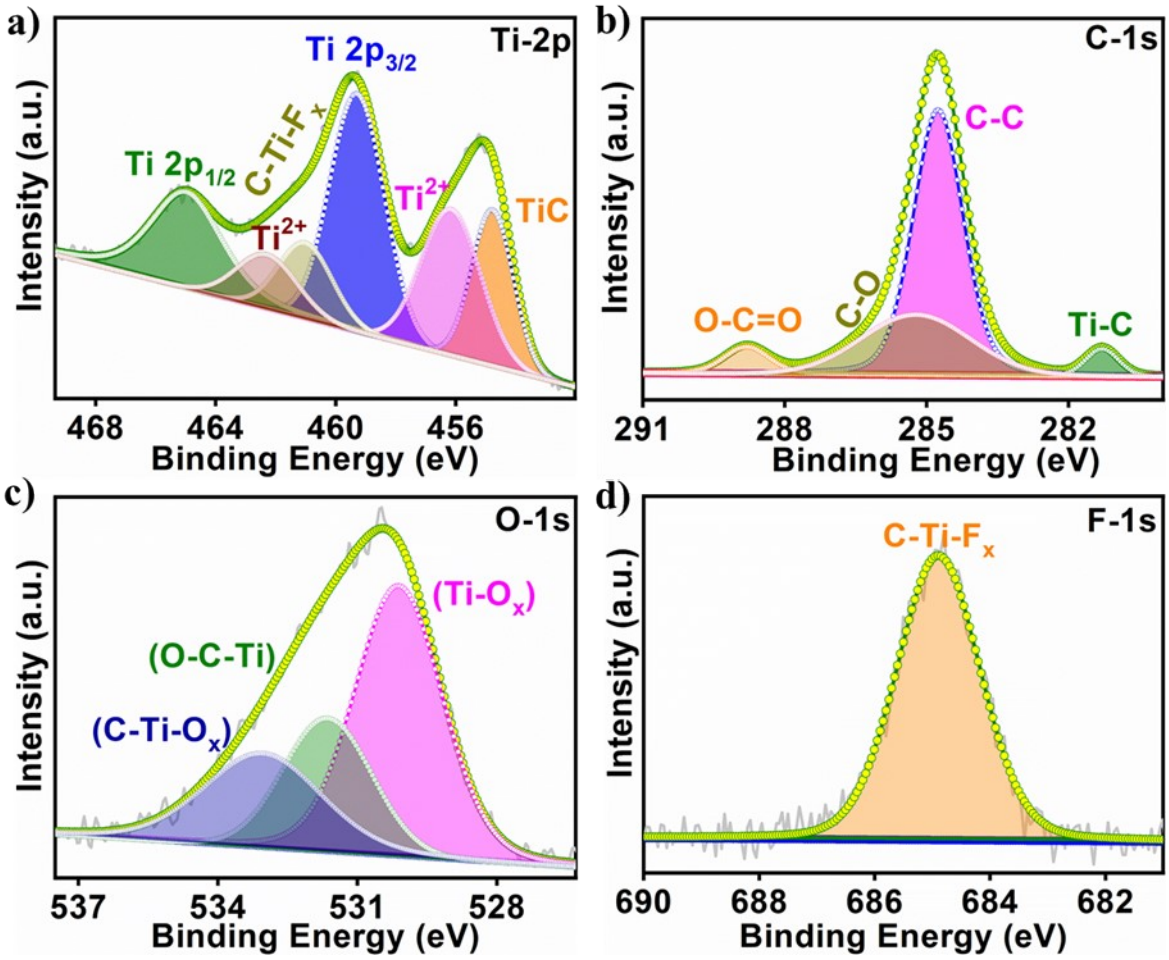

Figure S4. XP spectra (a) Ti 2p, (b) C 1s, (c) O 1s and (d) F 1s core levels of MXene ($Ti_3C_2T_x$).

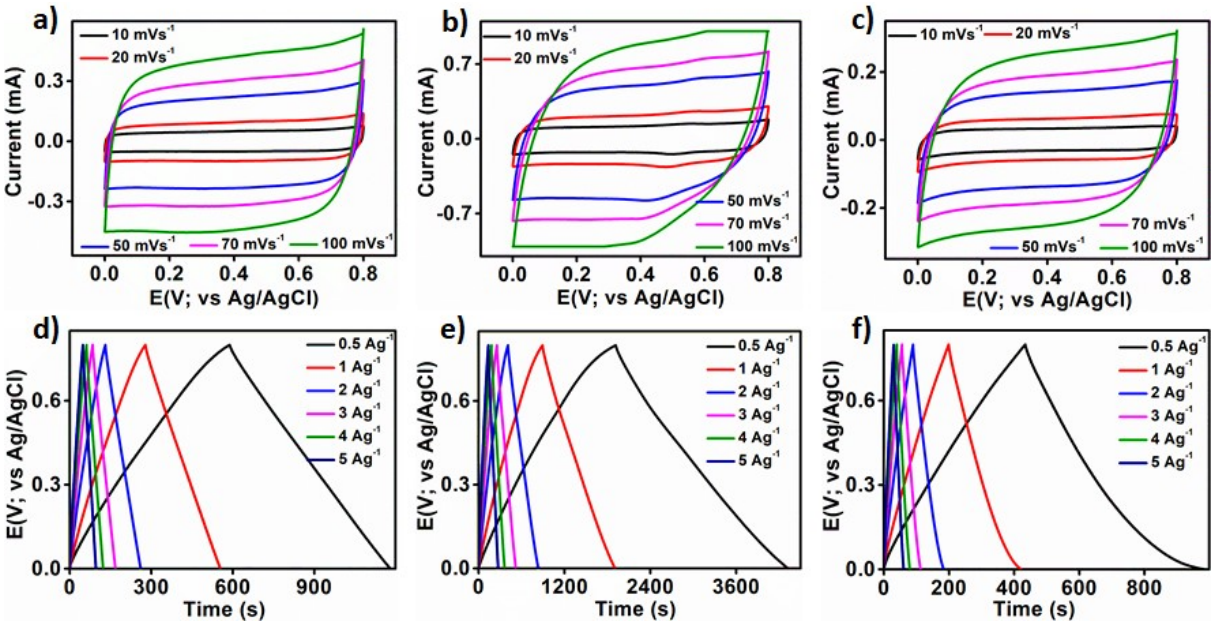

Figure S5. (a-c) CV and (d-f) GCD curves at various scan rates and current densities recorded for MC-900, MC-1000 and MC-1100 in 0.5 M H_2SO_4 acidic electrolyte.

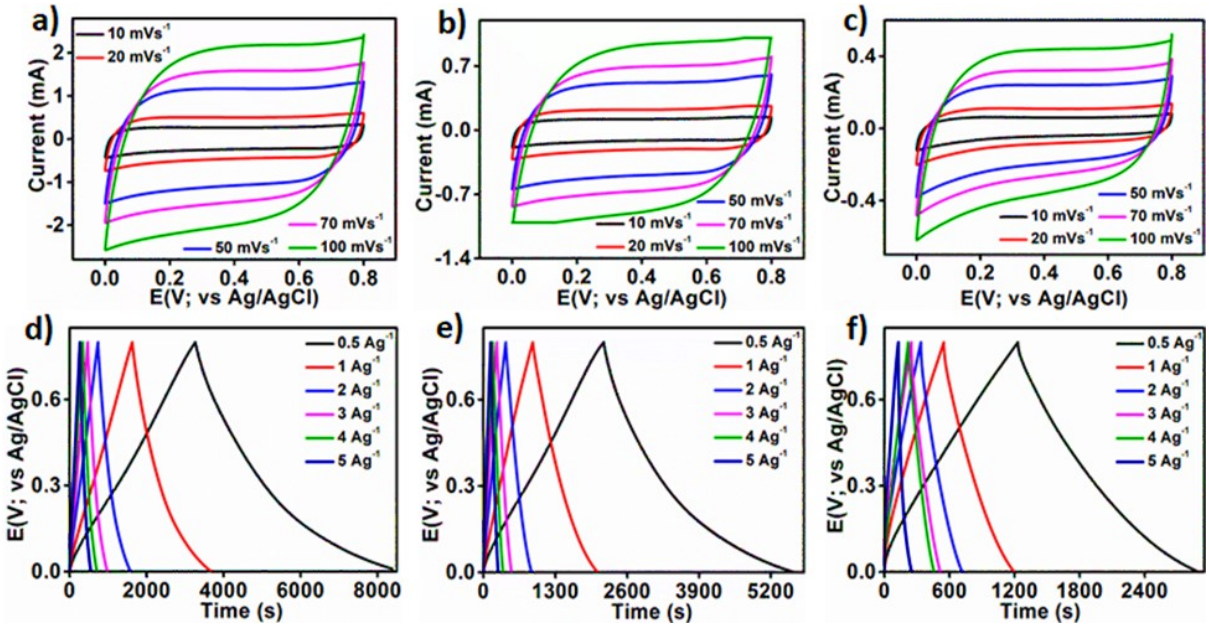

Figure S6. (a-c) CV and (d-e) GCD curves at various scan rates and current densities recorded for $Ti_3C_2T_x$/MC-9, $Ti_3C_2T_x$/MC-5 and $Ti_3C_2T_x$/MC-1 in 0.5 M H_2SO_4 acidic electrolyte.

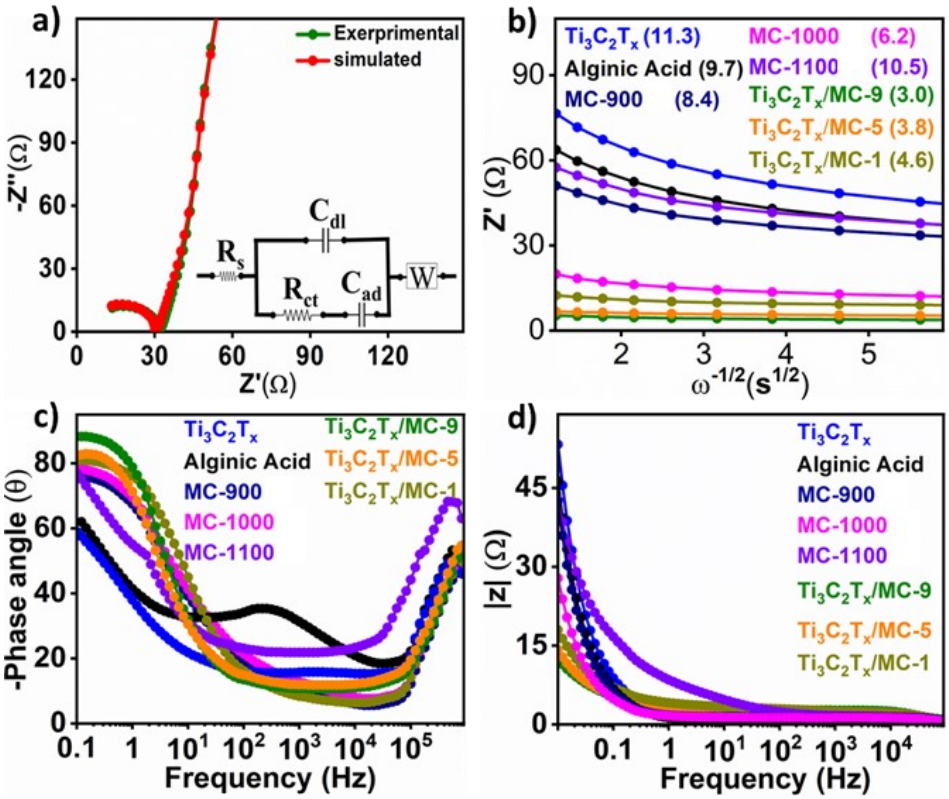

Figure S7. (a) Experimental and fitted EIS curves for $Ti_3C_2T_x$/MC-9 electrode and the inset shows corresponding equivalent circuit diagram; (b) linear fit of Z' data against the square root of the period (ω) in the high-frequency region; Bode plot (c) -phase angle vs. frequency, (d) |z| vs. frequency.

Table S2. The transport properties of various electrodes obtained from simulated impendence spectra in Fig. (6e and 6f).

Materials	**R_s(Ω)**	**R_{ct}(Ω)**	**Z_w(m Ω $s^{-1/2}$)**	**C_{ad} (mF)**
Alginic Acid	13.5	52.0	9.7	0.04
MC-900	13.5	45.5	8.4	0.03
MC-1000	12.8	39.1	6.2	0.6
MC-1100	13.4	50.1	10.5	0.9
$Ti_3C_2T_x$	15.4	56.1	11.3	0.06
$Ti_3C_2T_x$/MC-9	12.8	31.6	3.0	0.4
$Ti_3C_2T_x$/MC-5	12.8	34.1	3.8	0.6
$Ti_3C_2T_x$/MC-1	13.5	35.6	4.6	0.7

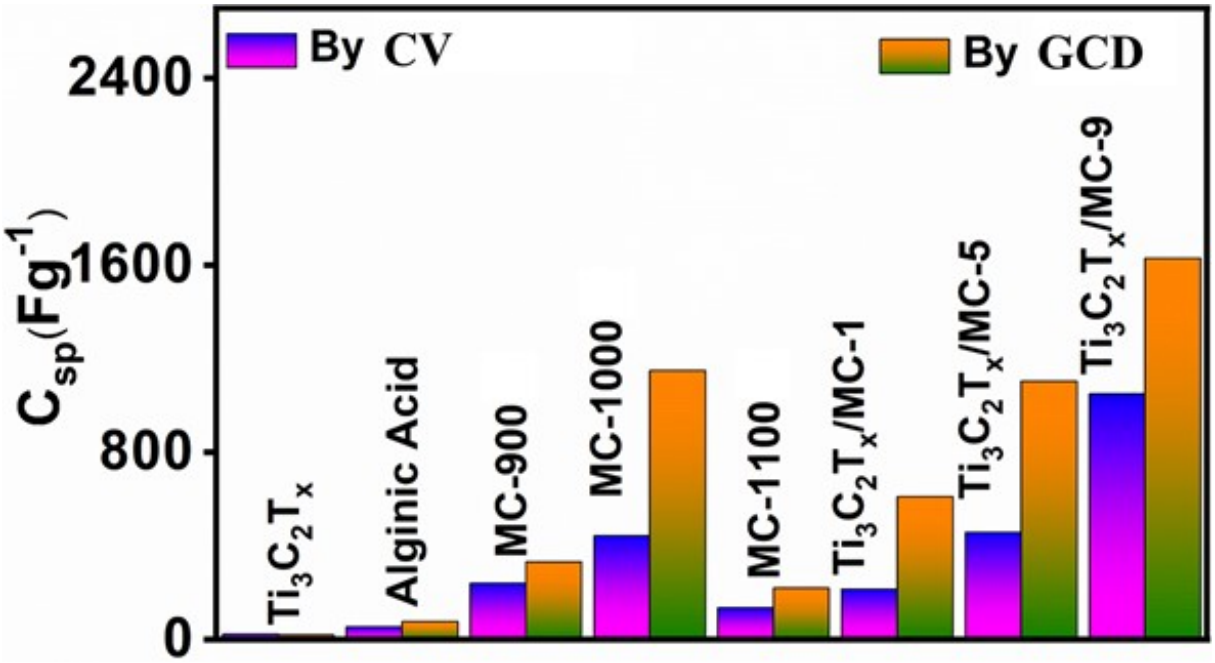

Figure S8. The specific capacitance for various synthesized nanocomposites from cyclic voltammetry (blue-pink bar) and galvanostatic charge-discharge (green-orange bar) at sweep rate and current density of 100 mV s^{-1} and 1 A g^{-1} respectively.

Table S3 The calculated specific capacitance in half-cell configuration for various active electrode materials.

Materials	**Specific Capacitance (F g^{-1})**	
	by CV @ scan rate of 100 mV s^{-1}	**by GCD** @ current density of 1 A g^{-1}
Alginic Acid	54	76
MC-900	240	331
MC-1000	442	1149
MC-1100	134	219
$Ti_3C_2T_x$	22	18
$Ti_3C_2T_x$/MC-9	1049	1629
$Ti_3C_2T_x$/MC-5	457	1102
$Ti_3C_2T_x$/MC-1	214	610

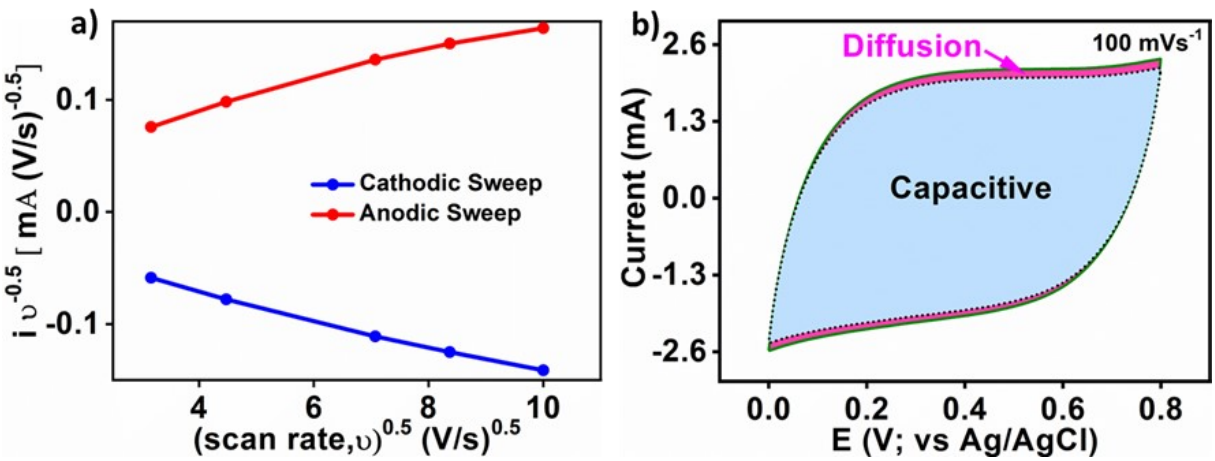

Figure S9. (a) The plot of i/(scan rate, ν)$^{0.5}$ against ν$^{0.5}$ for both anodic and cathodic voltammetric sweeps under an acidic medium to evaluate the value of k_1 and k_2 in equation 10 (from the main text); (b) CV curves at 100 mV s^{-1}, showing the surface and diffusion-controlled charge storage contributions.

Table S4. The calculated specific capacitance of $Ti_3C_2T_x$/MC-9 electrode material under the half-cell configuration.

Cycles No. (1K=1000)	**Specific Capacitance (F g^{-1})**	
	by CV @ scan rate of 100 mV s^{-1}	**by GCD** @ current density of 1 A g^{-1}
0k	1049	1629
5k	985	1484
10k	1017	1633
15k	1036	1627
20k	953	1629
25k	1051	1632
30k	1036	1640
35k	933	1627

Table S5. The calculated Specific Capacitance from CV and GCD curves of fabricated MC-1000//$Ti_3C_2T_x$/MC-9 asymmetric supercapacitor device.

Cycles No. (1K=1000)	**Specific capacitance (F g^{-1})**	
	by CV @ scan rate of 100 mV s^{-1}	**by GCD** @ current density of 1 A g^{-1}
0k	51.7	80.3
10k	47.8	71.4
20k	47.5	71.5
30k	48.6	76.1
40k	48.5	76.3
50k	50.1	80.3
60k	50.5	78.3

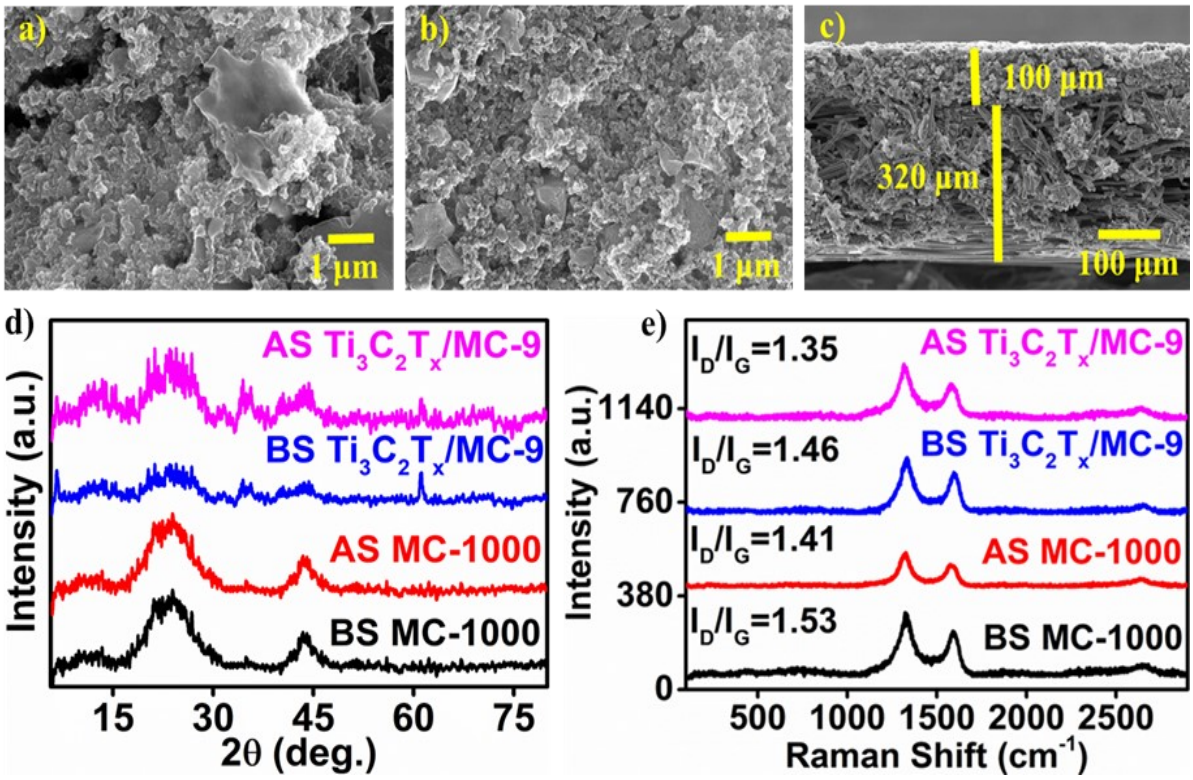

Figure S10. Post stability study of the Coin-Cell ASC; SEM images of (a-b) MC-1000, before and after stability, respectively; (c) SEM image displaying cross section of the $Ti_3C_2T_x$/MC-9 electrode material deposited on carbon paper showing its thickness; (d) XRD patterns and (e) Raman spectra of $Ti_3C_2T_x$/MC-9 and MC-1000, before and after stability study.

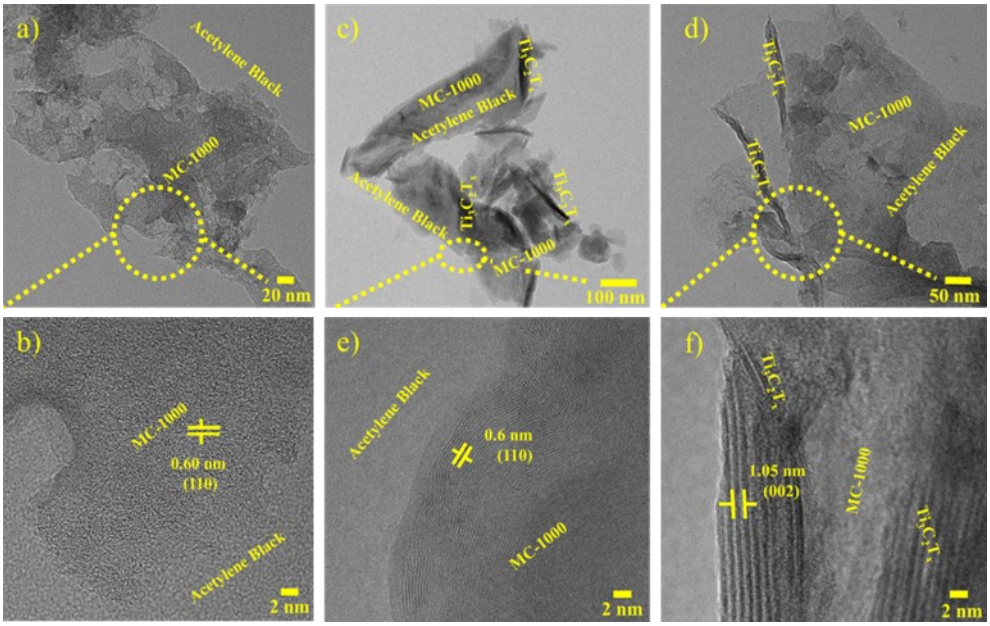

Figure S11. Post stability study: TEM and HRTEM images of (a-b) MC-1000 and (c-f) $Ti_3C_2T_x$/MC-9 nanocomposite.

Table S6. The comparative electrochemical performance for the MXene ($Ti_3C_2T_x$) and carbon based electrode materials.

Materials	Preparation Method	Electrolyte	Specific Capacitance		Cycling Stability[(a)]	Cycling Stability[(b)]	Ref.
			Electrode (a)	Device (b)			
CPCM/MXene	annealing treatment at 800°C	1mol/L H_2SO_4	362 F g^{-1}, 0.5 A g^{-1}	--	93.87 % @10,000	--	1
CP@rGO//MXene	oxidative polymerization	3 M H_2SO_4	280 F g^{-1}, 0.5 A g^{-1}	57, 59, and 47 F g^{-1},	--	88 % @20000 75 % @20000 80 % @10000	2
MXene/N-doped carbon foam	annealing treatment at 800°C	1M KOH	332 F g^{-1}	63 F g^{-1}	99.2 % @10,000	96 % @2500	3
$Ti_3C_2T_x$–MCNT	polymerization	0.5M Na_2SO_4	1.93 F cm^{-2}	0.94 F cm^{-2}	94 % @1000	72 % @1000	4
MXene-RuO_2	hydrothermal	1M H_2SO_4	388 F g^{-1}	93 F g^{-1}	88 % @20000	86 % @20000	5
$Ti_3C_2T_x$nanosheet /$Ti_3C_2T_x$QD/RGO	wet-spinning technique,	1m H_2SO_4	542 F cm^{-3}	53.1 F cm^{-3}	95.6 % @5,000	96.6 % @5000	6
$Ti_3C_2T_x$/RGO	hydrothermal	2M KOH	154.3 F g^{-1}	--	85 % @ 6,000	--	7
$Ti_3C_2T_x$/RGO	vacuum-assisted filtration	1M H_2SO_4	140 F g^{-1}	29 F g^{-1}	85 % @10,000	85 % @10,000	8
rGO: $Ti_3C_2T_x$	self-assembly 20000 rpm	1M H_2SO_4	254 F g^{-1} 2 mV s^{-1}	--	193 F g^{-1} @100 mVs^{-1}	---	9
MXene-rGO hydrogel	electrostatic self-assembly	3M H_2SO_4	320 F g^{-1}	--	46 % @8000	--	10
$Ti_3C_2T_x$-RGO	film through vacuum filtration	3M H_2SO_4	505 F g^{-1}	--	50 % @10,000	--	11
$Ti_3C_2T_x$/SCNT	Self-assembled composite film.	1M KOH	314 F cm^{-3}	--	95 % @10000	--	12
rGO/$Ti_3C_2T_x$	ultrasonic treatment calcined at 300°C	6M KOH	405 F g^{-1}	148.5 F g^{-1}	99.9 % @10,000	100 % @10,000	13

MXene/RGO	Ultrasonication After about 3 days,	1M H_2SO_4	233 F g^{-1}	--	91 % @ 10,000	--	14
Ti_3C_2/CNTs	EPD	6M KOH	134 F g^{-1}	55.3 F g^{-1}	@10000	--	15
3D porous MXene/rGO	300°C electric heating plates in a glove box	3M H_2SO_4	340.8 F g^{-1}	--	90.7 % @ 40,000	--	16
3D macroscopic graphene/MXene hydrogel	hydrothermal	6M KOH	267.7 F g^{-1}	--	100 % @10000	--	17
$Ti_3C_2T_x$/MC-9	**Solvothermal**	**0.5 M H_2SO_4**	**1629 F g^{-1} at 1 A g^{-1}**	**80.3 F g^{-1} at 1 A g^{-1}**	**99.9 % @35,000**	**97.5 % @60,000**	**This Work**

- CP = conducting Polymer
- CPCM = chitosan porous carbon Spheres
- Pin = Polyindole

References

1 L. Wei, W. Deng, S. Li, Z. Wu, J. Cai and J. Luo, *J. Bioresour. Bioprod.*, 2022, **7**, 63–72.

2 M. Boota and Y. Gogotsi, *Adv. Energy Mater.*, 2019, **9**, 1–8.

3 L. Sun, G. Song, Y. Sun, Q. Fu and C. Pan, *ACS Appl. Mater. Interfaces*, 2020, **12**, 44777–44788.

4 W. Liang and I. Zhitomirsky, *J. Mater. Chem. A*, 2021, **9**, 10335–10344.

5 C. Zhao, Q. Wang, H. Zhang, S. Passerini and X. Qian, *ACS Appl. Mater. Interfaces*, 2016, **8**, 15661–15667.

6 Y. Zhou, K. Maleski, B. Anasori, J. O. Thostenson, Y. Pang, Y. Feng, K. Zeng, C. B. Parker, S. Zauscher, Y. Gogotsi, J. T. Glass and C. Cao, *ACS Nano*, 2020, **14**, 3576–3586.

7 X. Zhou, Y. Qin, X. He, Q. Li, J. Sun, Z. Lei and Z.-H. Liu, *ACS Appl. Mater. Interfaces*, 2020, **12**, 11833–11842.

8 A. M. Navarro-Suárez, K. Maleski, T. Makaryan, J. Yan, B. Anasori and Y. Gogotsi, *Batter. Supercaps*, 2018, **1**, 33–38.

9 Q. Jiang, N. Kurra, M. Alhabeb, Y. Gogotsi and H. N. Alshareef, *Adv. Energy Mater.*, 2018, **8**, 1–10.

10 P. Dutta, A. Sikdar, A. Majumdar, M. Borah, N. Padma, S. Ghosh and U. N. Maiti, *Carbon N. Y.*, 2020, **169**, 225–234.

11 Q. Fu, X. Wang, N. Zhang, J. Wen, L. Li, H. Gao and X. Zhang, *J. Colloid Interface Sci.*, 2018, **511**, 128–134.

12 Y. Fang, B. Yang, D. He, H. Li, K. Zhu, L. Wu, K. Ye, K. Cheng, J. Yan, G. Wang and D. Cao, *Chinese Chem. Lett.*, 2020, **31**, 1004–1008.

13 L. Shao, J. Xu, J. Ma, B. Zhai, Y. Li, R. Xu, Z. Ma, G. Zhang, C. Wang and J. Qiu, *Compos. Commun.*, 2020, **19**, 108–113.

14 S. Xu, G. Wei, J. Li, W. Han and Y. Gogotsi, *J. Mater. Chem. A*, 2017, **5**, 17442–17451.

15 L. Yang, W. Zheng, P. Zhang, J. Chen, W. B. Tian, Y. M. Zhang and Z. M. Sun, *J. Electroanal. Chem.*, 2018, **830–831**, 1–6.

16 J. Miao, Q. Zhu, K. Li, P. Zhang, Q. Zhao and B. Xu, *J. Energy Chem.*, 2021, **52**, 243–250.

17 L. Zhang, S. W. Or, *APL Mater.* 2020, ***8***, 091101.